Pergamon

Acta Materialia •• (2001) •••–•••

Acta MATERIALIA

www.elsevier.com/locate/actamat

Kinetic modeling of phase selection during non-equilibrium solidification of a tungsten–carbon system

Marios D. Demetriou, Nasr M. Ghoniem *, Adrienne S. Lavine

Mechanical and Aerospace Engineering Department, University of California, Los Angeles, CA 90095-1597, USA

Received 10 September 2001;received in revised form 5 December 2001

Abstract

A dynamic computational model developed within the context of the classical theory of phase evolution was applied to the W–C system to simulate the kinetics of phase selection during non-equilibrium solidification at 50%-C between the thermodynamically stable WC and the metastable WC_{1-x} and W_2C. The kinetic variables used in the model are directly obtained from the free energy formulations that characterize the stable and metastable equilibria amongst participating phases. The isothermal kinetic analysis suggests that at low to moderate undercoolings, thermodynamic stability prevails, while at deep undercoolings (~1000 K) the crystallization of W_2C completes faster than the more thermodynamically stable WC_{1-x} and almost as fast as WC. The non-isothermal kinetic analysis suggests that thermodynamic stability prevails under moderate to high cooling rates (e.g. 10^4-10^6 K/s), however under ultra-high cooling rates (e.g. 10^8 K/s), the crystallization of WC_{1-x} and W_2C completes at nearly the same undercooling as that of WC.

Keywords: Rapid solidification; Plasma spray; Nucleation; Growth; Cluster dynamics

1. Introduction

The tungsten–carbon system is a refractory, compound-forming binary system. According to the constitution phase diagram investigated by Rudy [1], three different compounds are reported to form: a simple hexagonal carbide WC which melts incongruently and is almost stoichiometric, a cubic carbide which is referred to as WC_{1-x} and a second hexagonal carbide W_2C, both of which melt congruently and appear to have a slightly varying carbon content. The hexagonal WC–carbide, which appears to be the most preferred carbide, is stable from temperatures below room temperature up to 3049 K. WC is a refractory metal–carbide with good thermal and chemical stability, and is highly desirable since it combines high hardness, good oxidation resistance, a low coefficient of thermal expansion, a certain amount of plasticity, and good wettability by molten metals. The other two carbides, WC_{1-x} and W_2C, are not thermodynamically stable at room temperature and their formation in the final microstructure as metastable reaction byproducts is undesirable as it appears to promote brittleness and degrade wear resistance.

* Corresponding author. Tel.: +1-310-825-4866; fax: +1-310-206-4830.

E-mail address: ghoniem@ucla.edu (M.D. Demetriou).

1359-6454/01/$ - see front matter © 2001 Published by Elsevier Science Ltd on behalf of Acta Materialia Inc.
PII: S1359-6454(01)00447-5

In several rapid cooling experiments involving pure WC, such as splat quenching during thermal spraying or thin film deposition during laser cladding, the formation of WC_{1-x} and W_2C in the evolved microstructure was solely attributed to decarburization of WC at high temperatures [2–4]. The X-ray diffraction analysis of plasma-sprayed coatings obtained from pure WC powder presented by Sharafat et al. [5] is shown in Fig. 6. The analysis suggests that the final coating microstructure exhibits a spectrum of crystalline phases including, along with the stable WC phase, WC_{1-x}, W_2C, and W-solid-solution. The formation of W-rich phases may be attributed to the loss of carbon during processing, however, since neither WC_{1-x} nor W_2C are thermodynamically stable at room temperature, these phases are therefore metastable and decarburization cannot constitute a justification for their existence in the coating microstructure. Their formation should rather be attributed to metastability induced by non-equilibrium conditions that characterize rapid cooling processes.

In this study, a computational model is developed to assess the role of nucleation kinetics in the selection of kinetic path during annealing or upon continuous cooling at 50% carbon composition, which corresponds to the stoichiometric WC composition. The model, which was developed in the context of classical phase evolution theory, simulates the stochastic process of crystal nucleation by modeling the dynamics of cluster evolution and accounts for size-dependent growth. The kinetic variables used in the model were obtained directly from the free energy formulations that characterize the stable and metastable equilibria amongst participating phases. The nucleation-controlled phase selection process is evaluated by simulating the isothermal and non-isothermal kinetics of competing phases that crystallize via the corresponding stable and metastable triple point reactions. Consequently, the role of nucleation kinetics in obtaining a final microstructure that exhibits a spectrum of crystalline phases (such as the one shown in Fig. 1) rather than only WC is assessed. Since the aim of this study is to demonstrate that metastability may be a limiting factor in phase selection and consequently in microstructural evolution regardless of whether decarburization occurs, the model assumes fixed composition and neglects the loss of carbon.

2. Thermodynamic modeling

The kinetic analysis of metastability requires information about metastable thermodynamic equilibrium. According to Perepezko and Boettinger [6], metastable phase diagrams may be constructed by extrapolating the equilibrium phase boundaries into regions of metastability. Demetriou [7] developed a CALPHAD model to reproduce the stable W–C phase diagram in the composition vicinity of the carbides using free energy data from Gustafson's optimization [8]. He then extended the model to construct the metastable phase diagram by extrapolating the computed equilibrium boundaries into regions of metastability. The computed phase diagram in the vicinity of the three compounds is shown in Fig. 2. The stable phase equilibria, shown as solid lines, are in excellent agreement with those computed by Gustafson, which closely simulate Rudy's experimental phase equilibrium data. The metastable phase equilibria are shown as dotted lines. The thermodynamically stable and metastable reactions at 50%-C are tabulated in Table 1, along with the corresponding equilibrium compositions and temperatures. The reaction entropies associated with each of these triple-point transitions, ΔS_f, are computed from the free energy functions that characterize the participating phases and are also tabulated in Table 1.

From the phase diagram, the graphite liquidus temperature at 50%-C is ~3583 K. This is sufficiently higher than the peritectic temperature at ~3047 K, therefore the graphite phase is expected to crystallize adequately upon supercooling at 50%-C so that at the peritectic temperature an established equilibrium *liq–gra* interface may be assumed. At sufficiently large undercoolings, polymorphic WC nucleation via the metastable congruent reaction at ~3107 K will initiate, however, catalyzed WC nucleation originating along the existing *liq–gra* interface via the *liq* + *gra*→WC peritectic reaction is expected to dominate. At slightly larger undercoolings, catalyzed WC_{1-x} and W_2C nucleation will originate along the existing

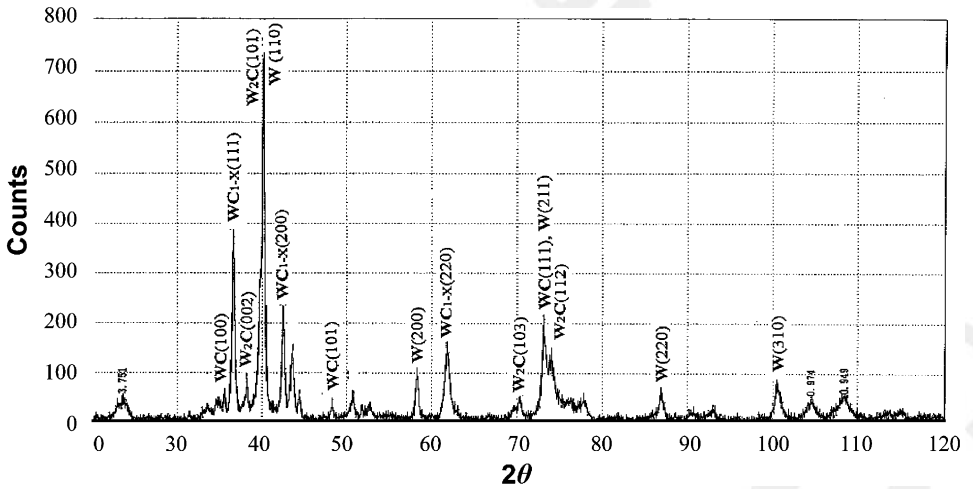

Fig. 1. X-ray diffraction analysis of a plasma-sprayed coating from pure WC powder [5].

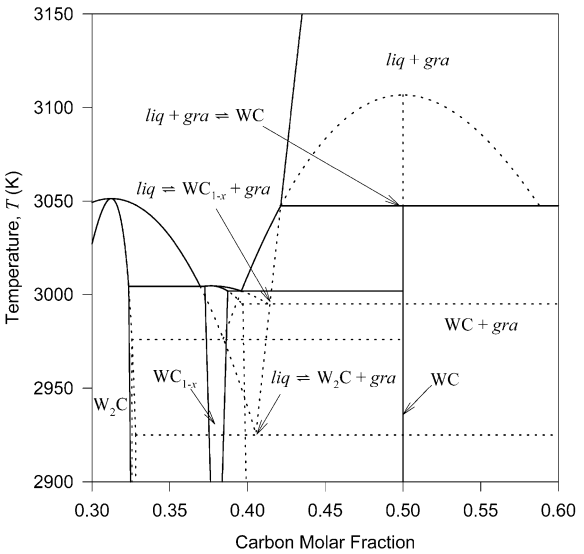

Fig. 2. The computed stable and metastable W–C phase diagram [7,8].

liq–gra interface via the *liq*→WC_{1-x} + *gra* and *liq*→W_2C + *gra* metastable eutectic reactions at ~2995 K and ~2925 K respectively. The non-equilibrium conditions that characterize rapid cooling processes are expected to induce substantially large undercoolings such that all three catalyzed nucleation reactions are sufficiently suppressed and a phase selection process unfolds.

For each nucleating phase, the degree of supersaturation $\Delta\mu$, which constitutes the driving force for the phase transition, is the free energy change associated with nucleating one molecule of product phase out of the parent medium [9]. The thermodynamic driving forces for nucleation of WC, WC_{1-x}, and W_2C out of the *liq–gra* equilibria are computed directly from the free energy formulations that characterize the participating phases and are plotted in Fig. 3. The $\Delta\mu$ vs. T plot, which quantifies the thermodynamic stability of each nucleating phase with reference to *liq–gra* equilibrium at 50%-C, suggests that WC has the largest driving force throughout the temperature range considered, while WC_{1-x} has a driving force larger than W_2C above 2500 K but smaller below.

3. Kinetic analysis

The criterion proposed by Hunziker et al. [10] for the formation of phases nucleating at triple points is adopted in this study. The criterion states that the nucleation density of the nucleating phase needs to be high enough such that the volume ahead of the growing interface is rapidly filled with the nucleating phase. Thus the kinetic analysis in this study will be conducted in terms of surface nucleation over established phase-interfaces, and the phase competition along the solidification pro-

Table 1
Phase equilibria of the competing stable and metastable reactions

Reaction	Reaction type	Carbon molar fraction			Temperature T (K)	Entropy of fusion ΔS_f (J/mol-K)
liq + *gra*⇄WC	Peritectic	0.421	0.500	1.00	3047	19.86
liq⇄WC_{1-x} + *gra*	Eutectic	0.396	0.414	1.00	2995	16.45
liq⇄W_2C + *gra*	Eutectic	0.328	0.406	1.00	2925	16.69

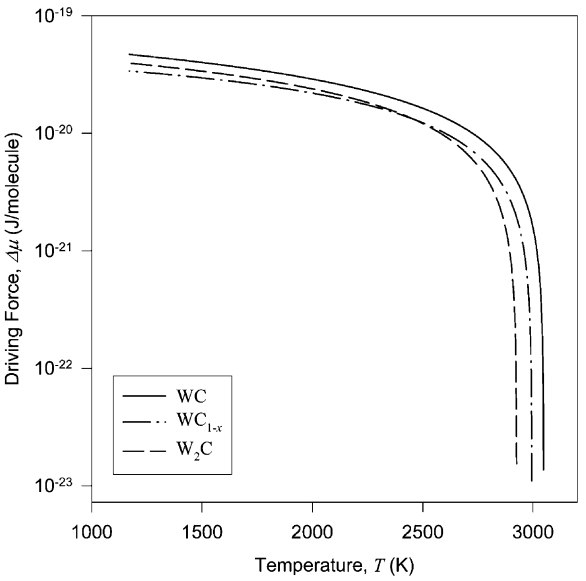

Fig. 3. Thermodynamic driving forces for WC, WC_{1-x}, and W_2C nucleation out of the *liq–gra* equilibria vs. temperature upon undercooling at 50%-C.

cess will be assessed by determining whether a nucleating phase has surface-crystallized substantially in relation to the competing phases.

For the solidification paths discussed above, i.e. peritectic and off eutectic, a metastable-equilibrium moving phase interface between the liquid and the primary solid (*gra*) is assumed to exist over which the nucleus of the secondary phase (WC, WC_{1-x}, or W_2C) emerges. This interface was treated as stationary during nucleation since its kinetics are limited by diffusion and are extremely slow compared to the rate-controlled kinetics of nucleating clusters. Owing to the strong interfacial tensions at the crystal–crystal interface, the emerging nucleus is expected to preferentially lie in the liquid. Furthermore, since atomic mobility in the liquid is anticipated to be significantly greater than in the solid, monomer transport is expected to occur predominantly in the liquid. Accordingly, for all reactions considered in the context of this study, the liquid is taken as the parent phase while the primary solid was treated as both stationary and inert and may be perceived as the substrate over which the nucleus is catalyzed. The geometry of a triple-point reaction modeled as a catalyzed reaction is illustrated in Fig. 4.

In catalyzed solidification reactions, the wetting angle θ can be correlated with the melting temperatures of the two participating solid phases [11], and for the nucleation of WC, WC_{1-x}, and W_2C, the wetting angles were evaluated to be 37°, 39°, and 38° respectively. The relationship between the size of a cluster of n molecules and its surface radius r, as shown in Fig. 4, is as follows:

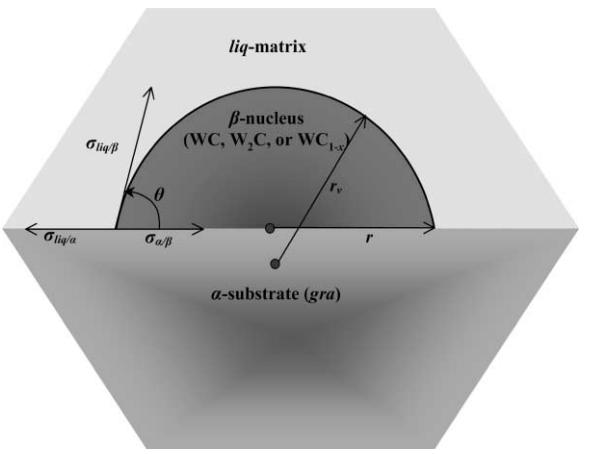

Fig. 4. The geometry of a triple point reaction: a β-phase (WC, W_2C, and WC_{1-x}) cluster nucleates in a *liq* matrix over an α-phase (*gra*) catalytic substrate.

$$r(n) = \sin\theta\left[\frac{3V_m}{4\pi f(\theta)}\right]^{1/3} n^{1/3} \quad (1)$$

where V_m is the molecular volume of the nucleating phase, and $f(\theta) = (2 + \cos\theta)(1-\cos\theta)^2/4$. The interface area of a cluster of n molecules is $A_n = (36\pi)^{1/3}[f(\theta)]^{1/3}V_m^{2/3}n^{2/3}$ while the number of sites on the cluster surface is $O_m = 2(1-\cos\theta)[f(\theta)]^{2/3}n^{2/3}$ [12]. The liquid-crystal interfacial energy for each nucleating phase is obtained from $\sigma_{liq/\beta} \equiv \sigma = \alpha_m \Delta S_f T/N_A V_m^{2/3}$ [9], where N_A is Avogadro's number, ΔS_f is the triple-point reaction entropy given in Table 1, and α_m is a structure dependent factor taken as 0.86.

The nucleating clusters for the phases considered in this study are taken to be stoichiometric, which is precise for WC but approximate for WC_{1-x} and W_2C, which were assumed to be at 33%-C and 40%-C stoichiometric compositions respectively. The cluster dimension can therefore be represented by a single size coordinate n, which would denote the number of stoichiometric molecules that make up the cluster. The availability of such stoichiometric units in the parent phase that would contribute to a unit surface of product phase, i.e. the initial surface density of available monomeric sites, can be approximated as $N^i \sim (fV_m)^{-2/3}$, where f is the phase fraction obtained from the lever rule. The molecular volume V_m is assumed to be the composition-weighted average of the molecular volumes of W and C, taken as 1.6×10^{-29} and 0.88×10^{-29} m^3/molecule respectively. In high-temperature nucleation reactions the mobility is high enough so that the barrier for stoichiometric units to diffuse from the bulk liquid to the cluster immediate vicinity is vanishingly small compared to the attachment/detachment interfacial barrier. Therefore, the cluster nearest-neighbor shell can be taken to have all of its sites O_n filled with stoichiometric molecules that attach/detach to the cluster stoichiometrically. Based on these assumptions, the current problem can be reduced to that of polymorphic nucleation, which can be modeled by the classical interface-limited cluster evolution theory.

The unbiased molecular jump frequency at the surface of a cluster may be approximated by the jump rate in the liquid. Assuming three-dimensional random walk process and the validity of Stokes–Einstein relationship, the jump rate γ can be related to the viscosity η as follows:

$$\gamma = \frac{2k_B T}{\pi V_m \eta} \quad (2)$$

where k_B is the Boltzmann's constant. The temperature dependent viscosity of the undercooled liquid was approximated using the isofree volume model proposed by Battezzati et al. [13], and the composition dependence was incorporated as suggested by Moelwyn-Hughes [14].

Fluctuation in the formation of an n-size cluster is connected with the minimum reversible work needed for its formation, which can be expressed as the balance between volume and surface contributions as follows [15]:

$$\Delta G_n = -n\Delta\mu + A_n\sigma \quad (3)$$

where macroscopic (independent of n) values for $\Delta\mu$ and σ are assumed. A maximum in ΔG_n is obtained at a critical size $n* = (32/3)\pi\sigma^3 V_m^2 f(\theta)/\Delta\mu^3$ as $\Delta G_{n*} = (16/3)\pi\sigma^3 V_m^2 f(\theta)/\Delta\mu^2$, and is referred to as the critical activation energy. The computed critical activation energies for nucleation of WC, WC_{1-x}, and W_2C are contrasted in Fig. 5, where the kinetic competition between the three phases is quantified. Fig. 5 reveals that above 2500 K WC has the lowest activation barrier, which implies that it is the most kinetically favored phase. However below 2500 K the activation barriers of both WC_{1-x} and W_2C appear to approach that of WC, hence WC_{1-x} and W_2C become nearly as kinetically favored as WC is.

4. Cluster dynamics

The cluster distribution function of an equilibrium system, whose homogeneous parent medium is equilibrated more rapidly than the formation time of the fluctuation, is obtained from fluctuation thermodynamics as $N_n^e = N^i \exp(-\Delta G_n/k_B T)$. This equilibrium cluster distribution function should satisfy detailed balance and render all fluxes zero, i.e.,

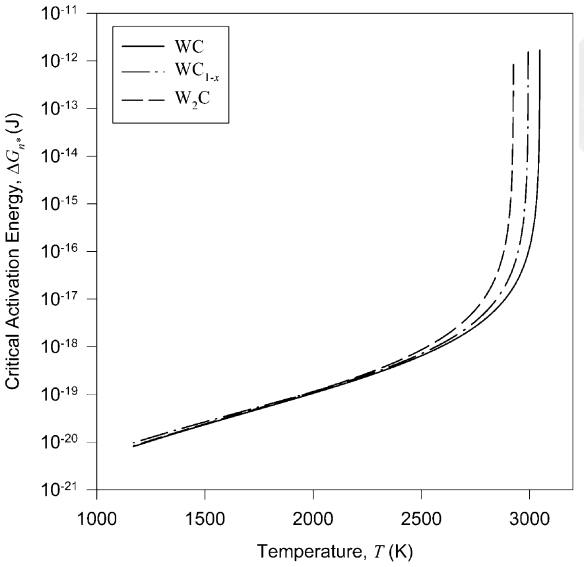

Fig. 5. The critical activation barriers for WC, W_2C, and WC_{1-x} nucleation during the reactions *liq* + *gra*→WC, *liq*→WC_{1-x}, and *liq*→W_2C + *gra*, respectively vs. temperature.

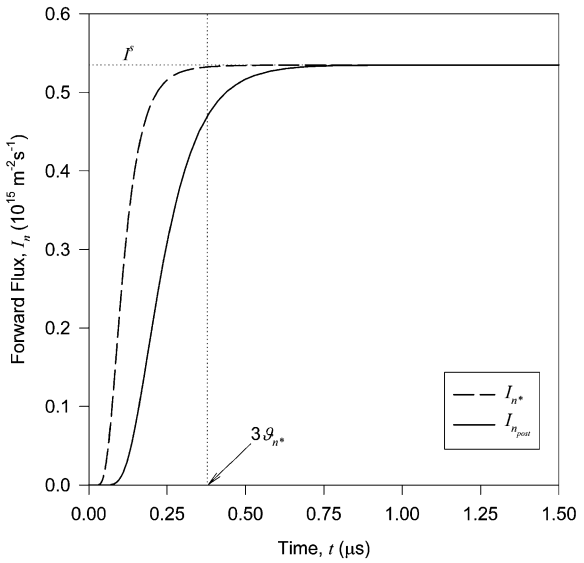

Fig. 6. Nucleation frequency of WC vs. time during annealing of the *liq* + *gra*→WC peritectic reaction at 2600 K for 1.5 μs.

$$N_n^{\mathrm{e}} k_n^+ = N_{n+1}^{\mathrm{e}} k_{n+1}^- \tag{4}$$

where k_n^+ is the rate of monomer attachment to an n-size cluster and k_n^- is the rate of monomer detachment. Considering also that the rate of attachment/detachment is proportional to $O_n\gamma$, the detailed balance Eq. (4) yields the rate constants [15]:

$$k_n^+ = O_n\gamma \exp\left(-\frac{\Delta G_{n+1} - \Delta G_n}{2k_{\mathrm{B}}T}\right) \tag{5a}$$

$$k_{n+1}^- = O_n\gamma \exp\left(-\frac{\Delta G_n - \Delta G_{n+1}}{2k_{\mathrm{B}}T}\right) \tag{5b}$$

According to the rate theory of atomic clustering, nucleation can be described as a random walk of nuclei in the space of their sizes and can be modeled by a first-order kinetic equation that has the form of a master equation, as follows [15]:

$$\frac{\mathrm{d}N_n(t)}{\mathrm{d}t} = N_{n-1}(t)k_{n-1}^+ - [N_n(t)k_n^- + N_n(t)k_n^+] + N_{n+1}(t)k_{n+1}^- \tag{6}$$

where $N_n(t)$ is the time dependent cluster density, and is determined from the solution to the system of stiff, coupled differential equations given by Eq. (6). Initially the cluster distribution assumes no preexisting clusters besides equilibrium configurations in the liquid up to a minimum size $n_{\min}$. During the simulation, the density of these minimum-size clusters, $N_{n_{\min}}(t)$, changes to reflect the depletion of monomers consumed during bimolecular reactions. Ideally, Eq. (6) must be solved for the entire size range $n_{\min} \leq n < \infty$. Due to computational limitations, however, the size boundary must be artificially truncated at an upper size $n_{\max}$. To ensure the accuracy of the simulation, this upper bound in size was chosen such that it sufficiently exceeded the critical size, i.e. $n_{\max} \gg n*$. The backward flux from clusters larger than this maximum size, $k_{n_{\max}+1}^-$, was taken to be zero, in effect assuming $N_{n_{\max}+1}(t) = 0$. A MATLAB stiff ODE solver calibrated to a relative tolerance of 10^{-3} was employed, which was supplied with the rate constants and with boundary and initial conditions and solved for the transient cluster size distribution.

The nucleation frequency at a cluster of size n,

$I_n(t)$, is the time-dependent flux past that size and is related to the time dependent cluster density $N_n(t)$ as follows:

$$I_n(t) = N_n(t)k_n^+ - N_{n+1}(t)k_{n+1}^- \quad (7)$$

During isothermal nucleation, a steady state cluster distribution would be established such that the nucleation rate becomes constant. This steady-state rate is given by:

$$I^s = \left(\sum_{n_{\min}}^{n_{\max}} \frac{1}{N_n^e k_n^+}\right)^{-1} \quad (8)$$

In the limit of n being continuous, the steady-state nucleation rate I^s and critical incubation time which may be regarded as the relaxation time ϑ_{n*}, were derived analytically as $I^s = zk_{n*}^+ N_{n*}^e$ and $\vartheta_{n*} 2/3\pi k_{n*}^+ z^2$, respectively, where $z = (\Delta\mu/6Gpk_B Tn*)^{1/2}$ is the Zeldovich factor [16].

For clusters sufficiently exceeding the critical size, the diffusion component of the nucleation rate that characterizes size fluctuations becomes vanishingly small in relation to the drift component that characterizes deterministic growth. Hence, ignoring fluctuational growth for $n \gg n*$, a growth law may be derived as $\dot{n} \cong I_n(t)/N_n(t)$, where $n \equiv dn/dt = k_n^+ - k_{n+1}^-$ is the drift velocity or growth rate. Utilizing Eqs. (1, 5a) and (5b), an initial value problem governing the time evolution of the surface radius of a supercritical cluster is derived as [7]:

$$\frac{dr}{dt} = \left(\frac{16V_m f(\theta)}{9\pi}\right)^{1/3} \sin\theta(1 - \cos\theta)\gamma \sinh\left(\frac{\Delta\mu - 2\sin\theta V_m\sigma/r}{2k_B T}\right) \quad (9)$$

In the limit of infinitely large crystals, Eq. (9) yields the size-independent crystal growth velocity $u = (dr/dt)|_{r\to\infty}$.

The time-dependent extended crystallized surface fraction, $x_e(t)$, can be established by accounting for the surface area of all supercritical clusters as follows:

$$x_e(t) = \sum_{n > n*} \pi[r(n)]^2 N_n(t) \quad (10)$$

Assuming that the transition from fluctuational to deterministic growth occurs at a post-critical size $n_{post} \gg n*$, the growth law may be utilized to transform the size summation into time integration as follows [7]:

$$x_e(t) = \int_0^t \pi[r(t;t')]^2 I_{r_{post}}(t')\, dt' \quad (11)$$

The convolution function $r(t;t')$ is the surface radius of a cluster at time t, which nucleated at a time t', and it represents the solution to the initial value problem given by Eq. (9). It characterizes the growth of a post-critical cluster from the nucleation time t', when $r(t') = r_{post}$, to the transformation time t. Under the assumption of zero-size nuclei and infinitely large crystals $r(t;t')$ becomes the convolution integral over the size-independent growth velocity u. Furthermore, taking the nucleation rate $I_{r_{post}}(t)$ to be relaxed at its steady state value I^s, a quasi-steady form of the kinetic problem may be obtained as follows:

$$x_e(t) = \int_0^t \pi\left[\int_{t'}^t u(t'')\, dt''\right]^2 I^s(t')\, dt' \quad (12)$$

Under isothermal conditions, the kinetics can be further reduced to:

$$x_e(t) = \frac{\pi}{3} I^s u^2 t^3 \quad (13)$$

The time-dependent surface fraction transformed that accounts for the overlap of crystallites is obtained from the Avrami statistical model [16] as follows:

$$x(t) = 1 - \exp[-x_e(t)] \quad (14)$$

According to the Avrami model, the time exponent in $x_e(t)$ (referred to as Avrami exponent) characterizes the dimensionality of the isothermal transformation, and for surface-nucleated two-dimensional crystallization this exponent must be ~3, in accordance with the current model.

5. Isothermal kinetics

The effects of nucleation transience during isothermal nucleation, which may be termed static,

become significant when the relaxation time ϑ_{n*} is comparable to the transformation time τ. A steady-state kinetic model neglects these transient effects and consequently overestimates the kinetics. In the work of Demetriou [7], the transient effects during isothermal nucleation for the reactions considered in this study were assessed by comparing the analytically-evaluated relaxation time to the transformation time evaluated from a steady state kinetic model, and were determined to be important when annealing below 2600 K. The isothermal transformation diagrams (TTT) are therefore produced by means of an explicit dynamic simulation of cluster evolution that accounts for nucleation transience and hence warrants the accuracy of the simulation at all annealing temperatures considered.

In the developed model, the duration of the isothermal anneal τ needs to be specified. The ODE solver then generates a large number of internal time intervals of exponentially varying duration over which the master equation that governs transient cluster evolution is solved and the formation rate of nuclei is calculated. Furthermore, the deterministic growth law is applied over the generated time intervals to solve for the growth of previously formed nuclei. The crystallized surface fraction is then computed by integrating the nucleation and subsequent growth of crystals over the transformation time as given by Eq. (11). For each simulated annealing, the duration to reach the onset of crystallization, taken to be $x = 10^{-6}$ (1-ppm) as suggested by Uhlmann [17], was recorded.

Crystallization of WC from the *liq* + gra→WC peritectic reaction will be considered as a sample case to illustrate the results for nucleation and growth during isothermal annealing at 2600 K. The annealing duration was taken to be $\tau = 1.5$ μs and the induction time at 2600 K was analytically computed as $\vartheta_{n*} = 0.125$ μs, about an order of magnitude smaller than τ. The time-dependent forward flux at n^* along with the one at n_{post} is plotted in Fig. 6. The forward flux at the critical size $I_{n^*}(t)$ appears to attain its steady-state value at $t \approx 3\vartheta_{n*}$, in accordance with the analytical treatment of Kashchiev [16]. The nucleation rate, which is taken to be the forward flux at the post-critical size $I_{n_{\text{post}}}(t)$, attains its steady-state value at $t \approx 6\vartheta_{n*}$. The time-dependent crystallized surface fraction $x(t)$ computed from dynamic and steady state models is plotted in Fig. 7. According to the dynamic model, 1-ppm crystallize at ~1.3 μs, while according to the steady state model, only ~0.3-ppm crystallize by that time. The steady state model, which is expected to be fairly accurate at early times since $\tau \gg \vartheta_{n*}$ at 2600 K, slightly underestimated the rate of crystallization at late times. This is because in evaluating growth in the steady state model the initial size of nuclei was ignored. For annealing below 2600 K though, $\tau \leq \vartheta_{n*}$ and the steady state model overestimates the kinetics. The TTT diagram for this transition computed from dynamic and steady state models is shown in Fig. 8, which illustrates the deviation between the two models and validates the analysis of transience based on time scale analogy.

The TTT diagrams produced by the dynamic model for WC, WC_{1-x}, and W_2C crystallization during the *liq* + *gra*→WC, *liq*→WC_{1-x} + *gra*, and *liq*→W_2C + *gra* solidification reactions respectively are superimposed in Fig. 9. The nose of the curve, which represents the temperature of the highest crystallization rate, occurs at ~2100 K for all three phases. At the nose temperature, WC

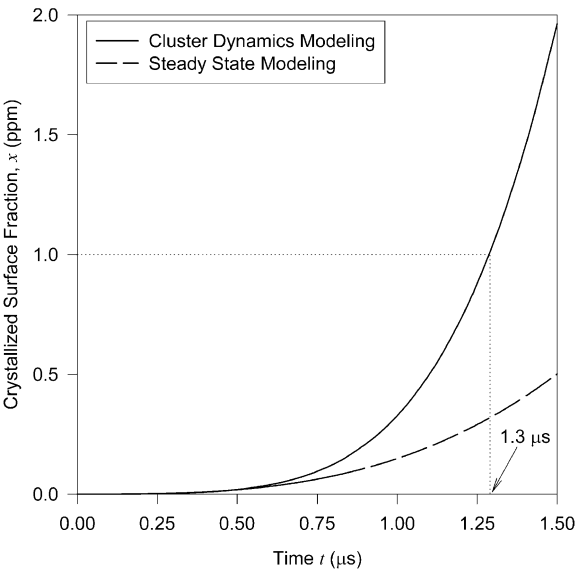

Fig. 7. Crystallized surface fraction of WC vs. time during annealing of the *liq* + *gra*→WC peritectic reaction at 2600 K for 1.5 μs.

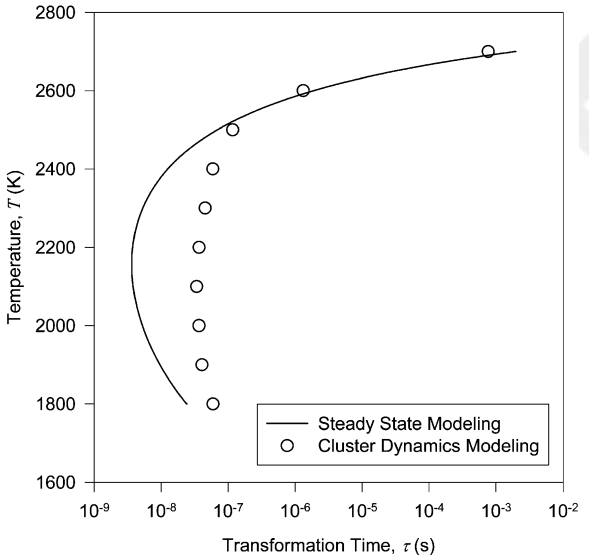

Fig. 8. Transient and steady-state TTT diagrams for WC crystallization during the peritectic reaction *liq* + *gra*→WC for $x = 10^{-6}$.

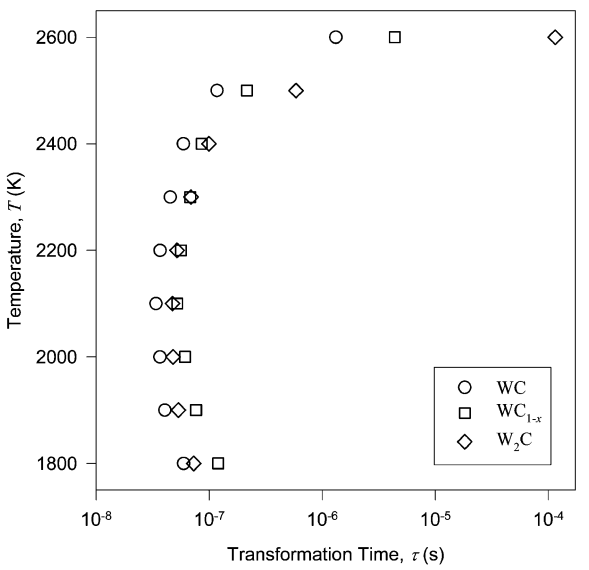

Fig. 9. Transient TTT diagrams for WC, WC_{1-x}, and W_2C crystallization during the reactions *liq* + *gra*→WC, *liq*→WC_{1-x}, and *liq*→W_2C + *gra*, respectively for $x = 10^{-6}$.

transforms in ~34 ns, WC_{1-x} in ~52 ns, and W_2C in ~47 ns. Assuming that no interaction between the competing phases has taken place at 1-ppm crystallization, Fig. 9 illustrates the phase competition during annealing at various temperatures. At temperatures sufficiently higher than the nose, the competing phases crystallize in an order that complies with thermodynamic stability, which states that WC is the most thermodynamically stable compound, followed by WC_{1-x} and the least thermodynamically stable is W_2C. However, at the nose temperature, the crystallization of W_2C completes faster than the more thermodynamically stable WC_{1-x} and at lower temperatures W_2C transforms as fast as WC, hence a high level of kinetic interference between WC and W_2C is anticipated at such deep undercoolings.

6. Non-isothermal kinetics

During non-isothermal transitions, dynamic effects attributed to the explicit dependence of the activation barrier on temperature may become significant when the activation barrier changes faster than the relaxation time to steady state [19]. The time scale characterizing the rate of change of the critical activation barrier is given by $\varphi_{n*} = [\mathrm{d}(-\Delta G_{n*}/k_B T)/\mathrm{d}t]^{-1}$ hence it is inversely proportional to the cooling rate. These dynamic effects become important when $\varphi_{n*} \ll \vartheta_{n*}$. In the work of Demetriou [7], the dynamic effects for the reactions considered in this study were assessed by comparing ϑ_{n*} to φ_{n*} for different cooling rates in the temperature range of the transition, and were determined to be important under ultra-high cooling rates such as 10^8 K/s. Therefore in order to warrant the simulation accuracy at all cooling rates considered, the non-isothermal crystallization kinetics were computed using the dynamic simulation.

The non-isothermal dynamic simulation adopted by Kelton and Greer [20] is employed, which directly simulates the dynamics of cluster formation and accounts for size-dependent growth of finite-size nuclei. In the employed simulation, the continuous non-isothermal process is divided into small isothermal anneals of equal duration over which new nuclei form and previously nucleated

ones grow. During each isothermal anneal, the ODE solver generates a large number of intermediate time intervals of exponentially varying duration over which the master equation is solved. At the end of each anneal, the density of nuclei generated during the annealing duration is stored and the sizes of nuclei generated in previous anneals are grown deterministically. In every new anneal the algorithm changes the temperature in accordance with the cooling rate and recalculates the rate constants. The calculation then continues using the new rate constants, starting with the distribution of clusters inherited from the previous anneal. As it is computationally infeasible to start the simulation at the equilibrium temperature, an appropriate initial temperature was determined by starting the simulation at temperatures successively closer to equilibrium until the crystallization kinetics were converged implying negligible contribution of nucleation and growth from the equilibrium to the initial temperature. Numerically, transience becomes a strong function of the annealing duration; therefore the isothermal duration must be adjusted so that dynamic effects are accounted for in a physical manner. For a given processing rate, the annealing duration was therefore adjusted to the shortest time scale that characterizes the barrier rate of change, i.e. to φ_{n*} evaluated at the initial temperature.

Crystallization of WC from the *liq* + *gra*→WC peritectic reaction will again be considered as a sample case to illustrate the results for non-isothermal nucleation and growth under 10^4, 10^6, and 10^8 K/s cooling rates. The transient nucleation frequency for different cooling rates is plotted within the corresponding transformation range along with the quasi-steady-state nucleation rate in Fig. 10. For processing rates of 10^4 and 10^6 K/s, the transient nucleation frequency appears indistinguishable from the quasi-steady-state rate, however for 10^8 K/s it deviates substantially, verifying the evaluation of transience based on time scale analogy. The crystallization kinetics computed from the dynamic simulation along with those computed from the QSS simulation for 10^4, 10^6, and 10^8 K/s cooling rates, are shown in Fig. 11. The dynamic results for 10^4 and 10^6 K/s cooling rates appear indistinguishable from the QSS ones for all nucleating phases, as dynamic effects for these rates are anticipated to be negligible and accounting for finite-size nuclei and size-dependent growth apparently had little effect. In the case of

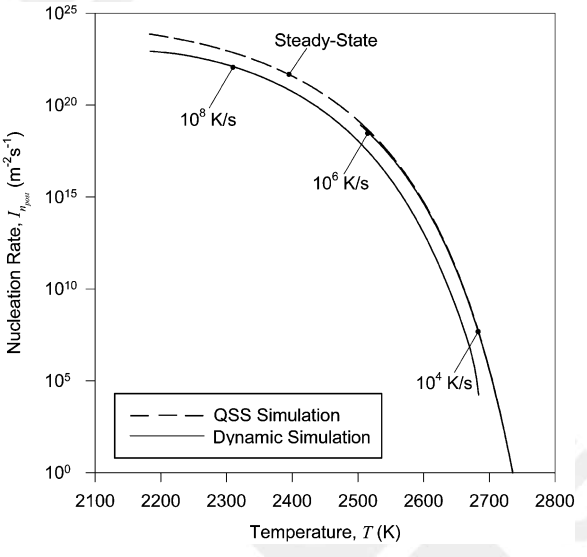

Fig. 10. Dynamic nucleation of WC during the *liq* + *gra*→WC peritectic reaction vs. temperature for various cooling rates.

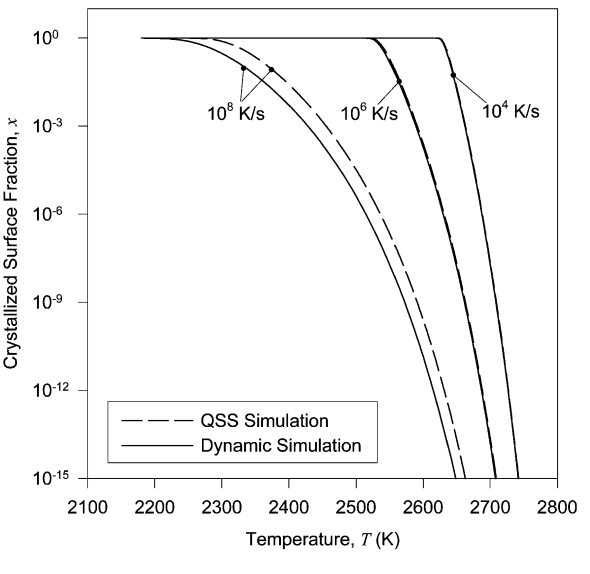

Fig. 11. Dynamic crystallization of WC during the *liq* + *gra*→WC peritectic reaction vs. temperature for various cooling rates.

10^8 K/s cooling rate, the kinetics computed by the dynamic simulation appear substantially slower than those computed by the QSS simulation, and according to the evaluation of non-isothermal transience based on time scale analogy, this difference should mainly be attributed to dynamic effects.

In order to demonstrate the dynamics of phase selection at different cooling rates, the kinetics of WC, WC_{1-x}, and W_2C during the *liq* + *gra*→WC, *liq*→WC_{1-x} + *gra*, and *liq*→W_2C + *gra* solidification reactions respectively for 10^4, 10^6, and 10^8 K/s cooling rates were contrasted in Fig. 12. In producing Fig. 12, the crystallization of each phase was computed by ignoring the kinetic interaction between competing phases, which can be a very good assumption at low crystallized fractions, however as x→1.0 it completely breaks down since cooperative growth needs to be taken into account. Therefore, at high crystallization, the phase competition illustrated in Fig. 12 does not portray the physical problem but it emphasizes the extent of kinetic interference between competing phases. Fig. 12 suggests that under all cooling rates considered, the competing phases crystallize in an order that complies with thermodynamic stability. Despite the fact that the kinetics of WC_{1-x} and W_2C appear to be faster than those of WC, thermodynamic stability prevails because in all cases the crystallization of WC initiated early enough so that it was completed first. At moderate cooling rates such as 10^4 K/s, the crystallization of WC is completed when the crystallization of the two other competing phases is negligible such that any kinetic interference is unlikely. At high cooling rates such as 10^6 K/s, the crystallization of WC is completed when the crystallization of the two other phases is small such that the level of kinetic interference, if any, would most likely be small. At ultra-high cooling rates such as 10^8 K/s, the suppression of all phases is extended to lower temperatures and consequently the crystallization of WC_{1-x} and W_2C is completed at nearly the same undercooling as that of WC.

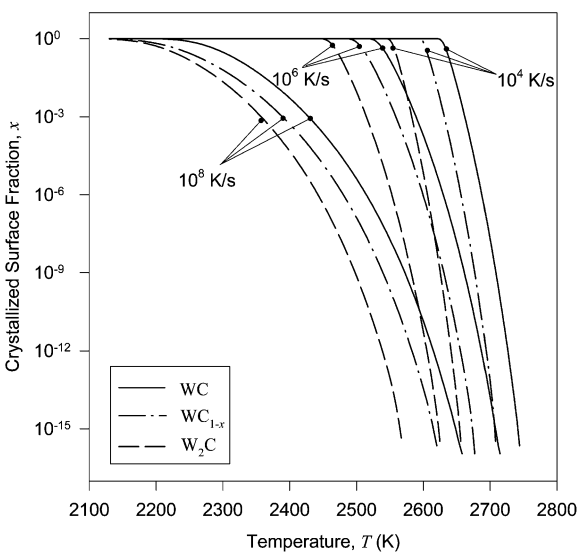

Fig. 12. Dynamic crystallization of WC during the *liq* + *gra*→WC, WC_{1-x}, and W_2C during the reactions *liq* + *gra*→WC, *liq*→WC_{1-x}, and *liq*→W_2C + *gra*, respectively vs. temperature for various cooling rates.

7. Conclusions

Microstructures obtained from rapid solidification of WC, like the one obtained by Sharafat et al. [5] presented in Fig. 1, appear to exhibit a spectrum of crystalline phases rather than only the stable WC. In this study, metastability is shown to constitute a limiting factor regardless of whether decarburization occurs. A simulation of the nucleation-controlled phase selection process was carried out in order to quantify the role of nucleation kinetics in microstructural evolution.

The conditions in this study are those encountered in rapid thermal processing of invariantly nucleating compound phases. A criterion for the formation of phases nucleating at a triple point is proposed by Hunziker et al. [10], which states that the nucleation density of the nucleating phase needs to be high enough such that the volume ahead of the growing interface is rapidly filled with the nucleating phase. This criterion was adopted in this study to assess the possibility for metastability by determining whether a compound has crystallized substantially in relation to the competing ones.

The isothermal kinetics suggest that at low to moderate undercoolings, thermodynamic stability

prevails, while at deep undercoolings (~1000 K) the crystallization of W_2C completes faster than the more thermodynamically stable WC_{1-x} and almost as fast as WC. The non-isothermal kinetics suggest that thermodynamic stability prevails under moderate to high cooling rates (e.g. 10^4–10^6 K/s), however under ultra-high cooling rates (e.g. 10^8 K/s), the crystallization of WC_{1-x} and W_2C completes at nearly the same undercooling as that of WC. Therefore under highly non-equilibrium conditions realized at deep undercoolings or upon rapid cooling, a high level of kinetic interference between the competing phases is anticipated, and cooperative growth between the phases may ensue during microstructural evolution such that all three, along with minor fractions of graphite, appear in the evolved microstructure.

Based on the model results, it is apparent that under highly non-equilibrium conditions the system cannot manage to kinetically respond to the induced deviation from equilibrium. The inadequacy in the system's kinetic response favors the prevalence of metastability and consequently thermodynamically favorable equilibration never manages to establish itself. Therefore, under non-equilibrium conditions encountered in rapid thermal processes such as splat quenching, metastability constitutes the limiting factor in the microstructural evolution regardless of whether decarburization occurs. Under the occurrence of decarburization, the average microstructural composition will be dictated by the loss of carbon during the process, however, as this study demonstrated, the phase selection and consequently the microstructure evolution will nevertheless be limited solely by kinetics.

8. Uncited reference

[18]

References

[1] Rudy E. Report AFML-TR-65-2, Part V, 1969, Wright–Patterson Air Force Base, OH.
[2] Tu D, Chang S, Chao C, Lin C. J Vac Sci Technol A 1985;3:2479.
[3] Verdon C, Karimi A, Martin J-L. Mater Sci Eng A 1998;A246:11.
[4] Suda Y, Nakazono T, Ebihara K, Baba K, Hatada R. Mater Chem Phys 1998;54:177.
[5] Sharafat S, Kobayashi A, Chen S, Ghoniem NM. Surf Coat Tech 2000;130:164.
[6] Perepezko JH, Boettinger WJ. Mater Res Soc Symp Proc 1983;19:223.
[7] Demetriou MD. Ph.D. dissertation, University of California, Los Angeles, 2001.
[8] Gustafson P. Mater Sci Tech 1986;2:653.
[9] Thompson CV, Spaepen F. Acta Metall 1983;31:2021.
[10] Hunziker O, Vandyoussefi M, Kurz W. Acta Mater 1998;18:6325.
[11] Eustathopoulos N, Pique D. Scripta Metall 1980;14:1291.
[12] Greer AL, Evans PV, Hamerton RG, Shangguan DK. J Cryst Growth 1990;99:38.
[13] Battezzati L, Antonione C, Riontino G. J Non-Cryst Solids 1987;89:114.
[14] Moelwyn-Hughes EA. Physical Chemistry. Oxford: Pergamon Press, 1964.
[15] Kelton KF, Greer AL, Thompson CV. J Chem Phys 1983;79:6261.
[16] Kashchiev D. Surf Sci 1969;14:209.
[17] Avrami M. J Chem Phys 1940;8:212.
[18] Uhlmann DR. J Non-Cryst Solids 1972;7:337.
[19] Shneidman VA. J Chem Phys 1995;103:9772.
[20] Kelton KF, Greer AL. J Non-Cryst Solids 1986;79:295.